PHYSICAL REVIEW B **75**, 125422 (2007)

Electronic structure of ultrathin γ'-Fe_4N (100) films epitaxially grown on Cu(100)

Cristina Navio,[1] Jesus Alvarez,[1] Maria Jose Capitan,[2] David Ecija,[1] Jose Maria Gallego,[3] Felix Yndurain,[1] and Rodolfo Miranda[1]

[1]*Departamento de Física de la Materia Condensada e Instituto Nicolas Cabrera, Universidad Autónoma de Madrid, Cantoblanco, 28049 Madrid, Spain*

[2]*Instituto de Estructura de la Materia-CSIC, 28006 Madrid, Spain*

[3]*Instituto de Ciencia de Materiales de Madrid-CSIC, Cantoblanco, 28049 Madrid, Spain*

(Received 9 June 2006; revised manuscript received 14 December 2006; published 22 March 2007)

The electronic structure of ultrathin films of γ'-Fe_4N(100) deposited on Cu(100) has been characterized by a combination of photoelectron spectroscopies, scanning tunneling microscopy, and diffraction techniques. The comparison of the data with first-principles simulations sheds light on magnetic moments, type of bonding, and charge transfer. N atoms residing in the bulk or at the surface are found to be distinguishable. The γ'-Fe_4N(100) surface is laterally heterogeneous and contains both areas reconstructed with a $p4gm(2\times2)$ symmetry and bulklike terminated. The densities of states of the reconstructed and unreconstructed areas of the surface are obtained and compared with the experiment. Comparison with $c(2\times2)$N/Fe(100) provides spectroscopic evidence that a subsurface excess of N drives the $p4gm(2\times2)$ reconstruction.

DOI: 10.1103/PhysRevB.75.125422 PACS number(s): 73.20.−r, 71.20.−b, 71.15.Mb, 68.37.Ef

I. INTRODUCTION

Recently, epitaxial films of magnetic iron nitrides[1] are raising renewed interest due to their chemically inert and mechanically hard surfaces, which, together with their intrinsic magnetic properties, make them suitable as magnetic layers alternative to pure Fe in devices such as reading heads.[2] In particular, thin epitaxial films of γ'-Fe_4N have been grown on MgO(001) (Refs. 3 and 4) or on Cu(100) (Refs. 5–7) with a high degree of structural perfection using a method based in molecular-beam epitaxy of Fe assisted with a radio-frequency source of atomic nitrogen. γ'-Fe_4N is a compound with well defined crystalline structure and magnetic properties. It is cubic with the Fe atoms forming a fcc sublattice, while the N atoms are placed at the bcc positions of the cubic cell, occupying one of the four octahedral hollow sites (see Fig. 2 below). Its lattice parameter is a=3.795 Å, i.e., expanded with respect to that of fcc Fe (a=3.45 Å). γ'-Fe_4N is ferromagnetic with a Curie temperature of 767 K and a saturation magnetization of 1.8 T.

There is general agreement in the magnetic properties of γ'-Fe_4N.[3,8] Surprisingly, its electronic structure is controversial. Previous calculations[9,10] disagree with respect to whether the bonding is covalent or ionic, the degree of charge transfer, or the magnetic moment. Experimental information on the electronic structure of γ'-Fe_4N is not yet available. In addition, γ'-Fe_4N(100) films present a $p4gm(2\times2)$ surface reconstruction, which has been proposed[7] to originate from a subsurface excess of N that would decouple electronically the surface layer from the bulk. This allows the two-dimensional interplay of magnetism and lattice instability that, in turn, would drive the reconstruction.

We report here on the electronic structure of carefully characterized γ'-Fe_4N(100) films carried out by means of a combination of experimental and theoretical techniques that allows us to determine the composition, crystallography, morphology, chemical bonding, core and valence-band states, and density of states (DOS). The study sheds some light on the nature of the chemical bonding and charge transfer, reveals the physics behind the type of surface reconstruction observed, and provides direct spectroscopic evidence for the existence of the subsurface N proposed to decouple the surface layer from the bulk and originate the reconstruction.

II. EXPERIMENTAL AND THEORETICAL METHODS

The experiments were performed in an ion-pumped ultrahigh-vacuum chamber with a base pressure of few times 10^{-10} mbar equipped with an x-ray source (Mg $K\alpha$, photon energy of 1253.6 eV), a discharge lamp which provides photons with energies of 21.22 eV (He I) and 40.8 eV (He II), electron and ion guns, and a low-energy electron-diffraction (LEED) optics. These sources allow us to perform x-ray photoelectron spectroscopy (XPS), ultraviolet photoelectron spectroscopy (UPS), and Auger electron spectroscopy (AES) using a hemispherical analyzer Leybold-Heraeus (LHS10) to detect the ejected electrons or ions. The spectrometer was calibrated with clean single-crystal samples to give the Cu $2p_{3/2}$ core level peak at 932.3 eV and the Fe $2p_{3/2}$ peak at 706.7 eV.

The substrate used for growing iron nitride films was a Cu(100) single crystal cleaned *in situ* by cycles of Ar^+ sputtering (1000 eV) and annealing at 900 K until no contamination was present in the XPS spectrum. The nitride films were grown by depositing Fe from a homemade evaporator at rates ranging from 0.001 to 1 ML/min (but mostly around 0.1 ML/min), while simultaneously exposing the substrate to a flux of atomic nitrogen obtained from a radio-frequency (rf) plasma discharge source.[11] The rf source employed a 1:1 mixture of nitrogen and hydrogen with an internal pressure of 10^{-2} mbar. The applied power was 6 W. The gas from the plasma container was directed to the substrate by means of a retractable tube, Teflon coated on the inside to reduce the recombination of N atoms. In these conditions, the pressure in the UHV chamber was 10^{-7} mbar and the efficiency in the

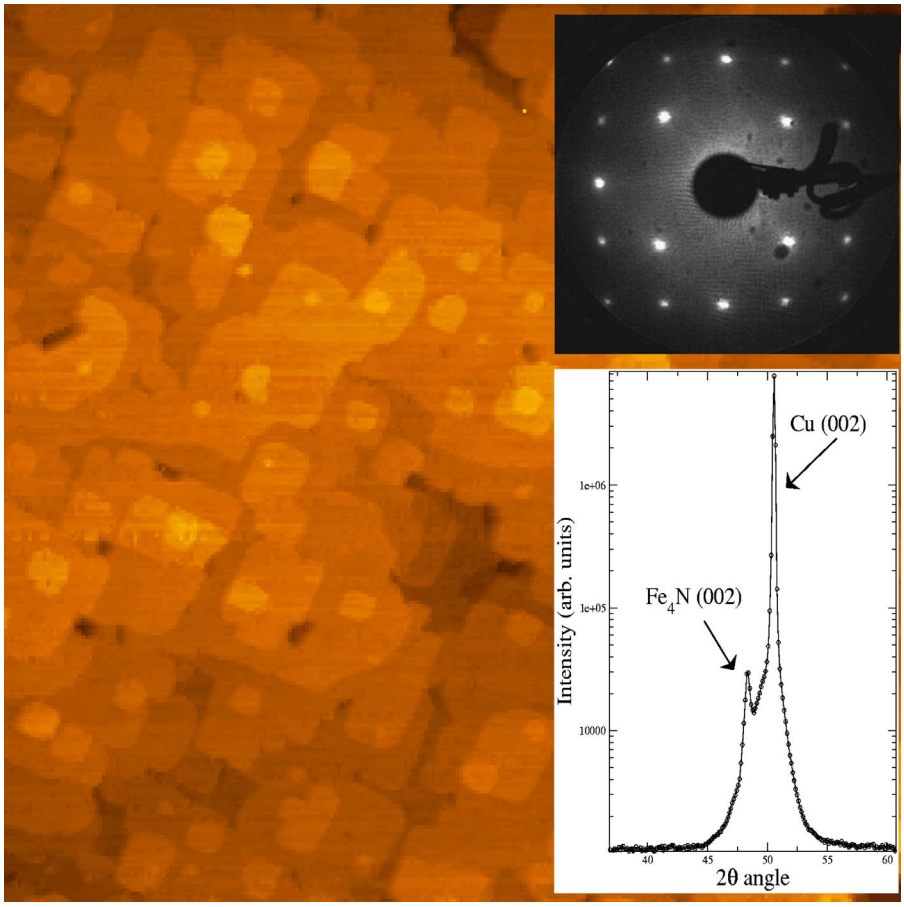

FIG. 1. (Color online) 3000×3000 Å^2 wide STM image of a 18-Å-thick γ'-Fe_4N film grown on Cu(100) at 700 K. The bias voltage was 0.35 V and the tunnel current was 0.47 nA. The image was recorded at 300 K. The upper inset shows the LEED pattern of the $p4gm(2\times2)$ reconstruction. The lower inset shows the x-ray diffraction pattern of the film with the (002) reflection of γ'-Fe_4N.

production of atomic N was 10%. During the growth, the substrate was kept at a temperature of 665–700 K, and the pressure in the UHV chamber was 5×10^{-7} mbar.

The scanning tunneling microscopy (STM) measurements were carried out in a separate chamber equipped with an identical rf source, after cooling the sample to 300 K. From earlier work, we know that high-temperature conditions result in the growth of epitaxial γ'-Fe_4N films on Cu(100) substrates.[6]

The experimental results were compared with first-principles, theoretical calculations performed in the context of density-functional theory[12] using the SIESTA (Ref. 13) method. For the exchange-correlation potential, we adopt a generalized gradient approximation.[14] The norm conserving pseudopotentials used follow the Troullier-Martins scheme[15] in the nonlocal form proposed by Kleinman and Bylander[16] and with partial core corrections.

III. RESULTS AND DISCUSSION

A. Growth of γ'-Fe_4N: Morphology, crystalline structure, and stoichiometry

The surface morphology of the γ'-Fe_4N film formed after exposing the Cu(100) substrate at 700 K to the N plasma and the beam of Fe is shown in Fig. 1. The large-scale STM image shows a rather smooth growth front. The film is continuous and consists of layers with square symmetry that contains islands of the next layer, displaying clearly the square symmetry of the crystalline structure. The measured step height is 1.9 Å, i.e., half the lattice parameter of γ'-Fe_4N. Only few layers are exposed simultaneously. The growth takes place in an (imperfect) layer-by-layer mode. At this large scale, the surface looks homogeneous. As shown previously,[6] the γ'-$Fe_4N(100)$ surface is reconstructed with $p4gm(2\times2)$ symmetry with respect to the substrate. The LEED pattern observed is shown in the upper inset and reflects the characteristic absence of the four first half-order spots of a simple 2×2 pattern typical of the $p4gm$ symmetry.[17]

The lower inset in Fig. 1 shows the *ex situ* x-ray diffraction pattern,[18] proving that the films have indeed the crystalline structure of γ'-Fe_4N. The diffractogram not only excludes the presence of other iron nitride phases but also indicates that the films are (100) oriented.

Figure 2 shows that there are two inequivalent Fe atoms in the crystalline structure of γ'-Fe_4N. The Fe I atoms, located at the corners of the cubic unit cell, are bonded to 12 Fe atoms as in fcc Fe. The Fe II atoms occupy the center of the faces and are bonded to Fe atoms *and* also to two N

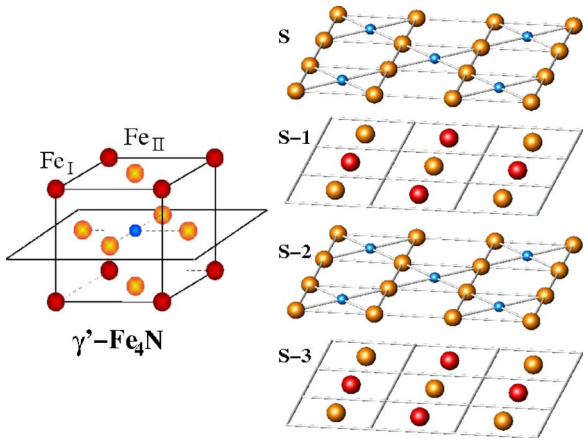

FIG. 2. (Color online) Crystalline structure of γ'-Fe_4N. The smaller (blue) spheres represent the N atoms, while the larger (red and yellow) spheres are the Fe atoms. Fe I atoms (not bonded to N) are shown yellow, light shaded, and Fe II (bonded to N) are shown red, dark shaded. The right part shows the atomic structure of the first four layers of bulk-terminated γ'-$Fe_4N(100)$ with the same color code.

atoms. The right part of Fig. 2 shows the crystalline structure of γ'-Fe_4N along the (100) direction, which consists of alternating planes of Fe_2N and pure Fe_2. Notice that the symmetry and atomic arrangements of the first two layers (S and S-1) are identical to those of the $c(2\times2)$ structure of N on Fe(100) and that the main difference between $c(2\times2)$N/Fe(100) and γ'-$Fe_4N(100)$, in the first four atomic layers, is the presence of N in the third layer (S-2) of γ'-Fe_4N.

The chemical characterization and the determination of the stoichiometry and the thickness of the grown films were carried out by XPS. X-ray reflectivity measurements also confirmed the thickness assigned to each film from the attenuation of the XPS peaks. Figures 3(b) and 4(b) show, respectively, the Fe $2p$ and N $1s$ core levels of a 15-Å-thick film. The peaks, after subtraction of the background, were fitted with standard line shapes.[19] Since all the Fe and N atoms in the films are within the escape depth of photoelectrons, the ratio of the Fe $2p_{3/2}$ and N $1s$ peak areas can be used to determine the average composition of the films following standard procedures[20] and using the atomic sensitivities determined previously for this particular spectrometer.[21] The resulting stoichiometry is $Fe_{4.0\pm0.2}N$. All films prepared in the reported conditions within the explored thickness range (10–30 Å) present the same composition, which is in agreement with the rather strict stoichiometry of γ'-Fe_4N. The Cu $2p$ spectra recorded through the nitride film (not shown) are identical to those of clean Cu(100), indicating that the substrate is not participating in the reaction or otherwise affected by the formation of the iron nitride films.

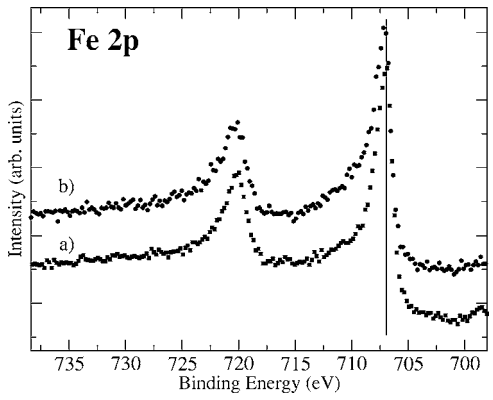

FIG. 3. Fe $2p$ core level of (a) $c(2\times2)$N/Fe(100) and (b) a 14-Å-thick γ'-Fe_4N film grown at 665 K on Cu(100).

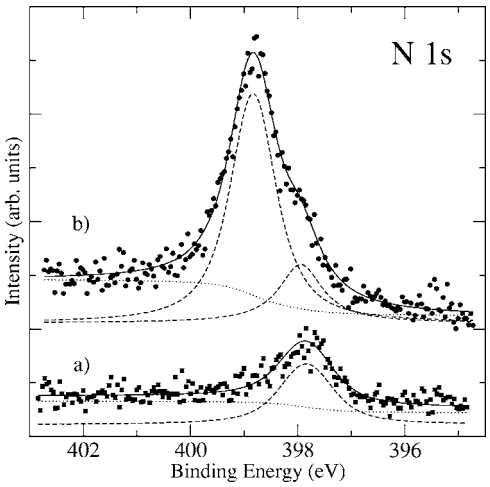

FIG. 4. N1s core levels of (a) $c(2\times2)$N/Fe(100 and (b) a 14-Å-thick γ'-Fe_4N film grown at 665 K on Cu(100). The dotted lines are the corresponding fits (see the text).

B. Electronic structure of γ'-$Fe_4N(100)$

The upper panels of Fig. 5 show the spin-split, valence-band DOS of bulk γ'-Fe_4N, projected on Fe I and II atoms. In our first-principles calculations, bulk Fe I atoms carry a total charge of 7.76 electrons and a *very large* magnetic moment (2.99 Bohr magnetons). Notice that this is similar to the one predicted for *expanded*, *high spin* fcc Fe (2.65 Bohr magnetons)[10] and much larger than the one of bcc Fe (2.25 Bohr magnetons). In our calculations, the Fe II atoms carry a *larger* total charge (7.9 electrons) and have a smaller (2.39 Bohr magnetons) magnetic moment. Early neutron diffraction data[22] and calculations[10] indicate the existence of different magnetic moments for Fe I (2.9–2.7 Bohr magnetons) and Fe II (2 Bohr magnetons) in γ'-Fe_4N.

Figure 5(a) shows an enhanced DOS in the region 6–8 eV below the Fermi level that reveals the bonding to N. Surprisingly, the ionic charge is larger in Fe I (0.24 electron) than in Fe II (0.1 electron), i.e., the atoms which are further away from N transfer more charge per atom. In any case, the total charge transfer is small and the bonding in γ'-Fe_4N is mostly covalent. Previous calculations have predicted the opposite[10] and, accordingly, the Fe $2p_{3/2}$ core levels of Fe I and II were calculated to differ by 0.75 eV,[9] with the one corresponding to Fe II shifted to higher binding energy (BE). Contrary to that prediction, the Fe $2p$ spectrum of Fig. 3(b) does not show hints of the presence of two components. The peak for γ'-Fe_4N is simply shifted 0.2 eV to higher BE (and

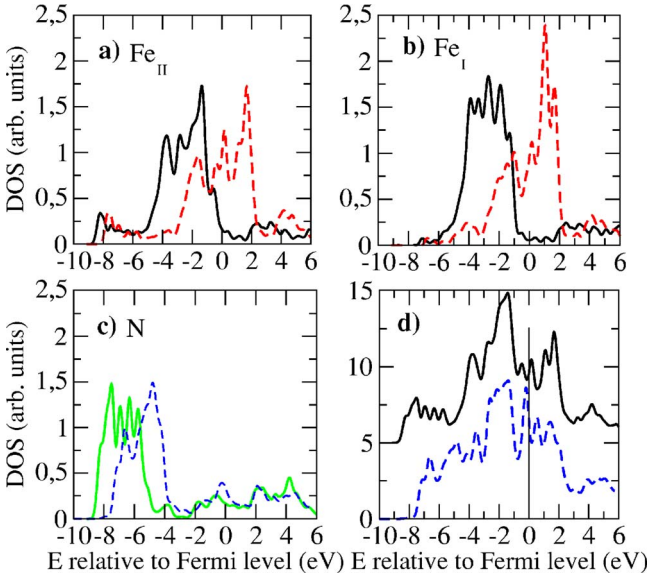

FIG. 5. (Color online) The two upper panels show the calculated DOS of bulk γ'-Fe_4N projected on (a) Fe II and (b) Fe I atoms. The black continuous (red broken) lines are the spin-up (down) contributions. Panel (c) shows the local DOS on the N atoms in the bulk (green continuous line) and at the surface (blue broken line). Panel (d) shows the calculated bulk total DOS (black upper line) and the DOS at the (100) surface of γ'-Fe_4N (blue broken line).

presents a slightly larger asymmetry in the line shape) with respect to the one of the $c(2\times2)$N/Fe(100) surface [Fig. 3(a)]. This confirms the small charge transfer per Fe atom to N and the covalent bonding indicated by our calculations.

Figure 5(c) shows a noticeable difference in the binding energy of the $2p$ valence levels for N atoms in the bulk and at the surface, although the total ionic charge per N atoms is almost identical (0.55 vs 0.53 electron, respectively). The surface N $2p$ level peaks at −5 eV and it is shifted to lower binding energies with respect to the bulk N $2p$ level at around 7 eV. The calculated excess charge of a N atom in the bulk with respect to isolated N (0.55 electron) is also much smaller than in previous calculations, which range from 1.4 (Ref. 10) to 1.08 electrons.[9]

The N $1s$ core level spectra of Fig. 4(b) display a main peak at a BE of 398.8 eV and a well defined shoulder on the low binding energy side of the photoemission line (397.9 eV). The main peak is assigned to N in the bulk of γ'-Fe_4N. The lower BE component is assigned to N atoms in the surface region, which have also the shifted N $2p$ valence level shown in Fig. 5(c). Note that the fit in Fig. 4(b) proves that the lower BE component of the N $1s$ peak of γ'-Fe_4N appears at the same energy (397.9 eV) and with the same line shape as that of surface N atoms in the $c(2\times2)$N/Fe(100) adlayer shown in Fig. 4(a). The difference in BE (0.9 eV) between the two N $1s$ components has been ascribed before[9] to the difference in ionic charge (0.25 electron per atom) between N atoms in the bulk and at the surface. This is not supported by our calculations.

Figure 5(d) also shows the calculated total DOS for a bulk crystal of γ'-Fe_4N and the DOS projected on the unreconstructed (100) surface. Note the high DOS at the Fermi energy of γ'-Fe_4N(100) predicted by the calculations. This suggests that this surface could be prone to reconstructions that would reduce the DOS at the Fermi level, as observed experimentally.[6,7]

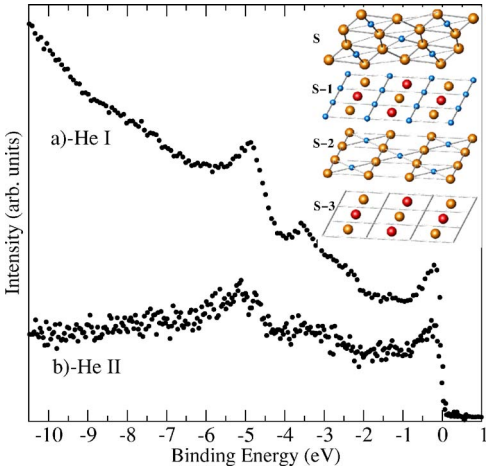

FIG. 6. (Color online) UPS recorded with He I and He II photons on a 13-Å-thick γ'-Fe_4N film grown at 665 K on Cu(100). The inset shows the crystalline structure of the first four layers of γ'-Fe_4N(100) with the $p4gm$ reconstruction due to excess N in the subsurface layer.

C. Electronic structure of the $p4gm$ reconstructed γ'-Fe_4N(100) surface

The (100) surface of γ'-Fe_4N is reconstructed with a $p4gm(2\times2)$ pattern with respect to the Cu(100) substrate. The atomic arrangement has been unraveled and a possible mechanism for the reconstruction has been recently proposed.[7] The mechanism requires the existence of subsurface excess of N, which would decouple electronically the surface from the bulk, thereby inducing a magnetically driven surface reconstruction with the observed $p4gm(2\times2)$ symmetry. The inset in Fig. 6 shows the proposed atomic model of the layer structure associated with the $p4gm$ reconstruction. Notice that the S-1 layer is now saturated with N and it has a Fe_2N_2 composition.

We have carried out first-principles calculations on a slab that contains a subsurface N-saturated layer. The simulation reproduces the reconstruction and indicates that both the total ionic charge (5.56 versus 5.61 electrons per atom) and the energy position of the valence-band N $2p$ levels (not shown) for N atoms in the surface (S) and subsurface (S-1) layers are almost identical. That is, they can hardly be distinguished spectroscopically on a $p4gm(2\times2)$ γ'-Fe_4N(100) sample.

The angle-integrated UPS spectra recorded on the same γ'-Fe_4N(100) film with photons of 21.2 and 40.8 eV are shown in Fig. 6. Both UPS spectra show a peak at −0.2 eV and other structures at −1.4, −2.5, and −3.5 eV. Note that the surface N $2p$ level at −5 eV is clearly seen and is *also* detected with He II photons. The $2p$ levels of N atoms in the bulk appear at −7.7 eV, in excellent agreement with the calculations shown in Fig. 5(c).

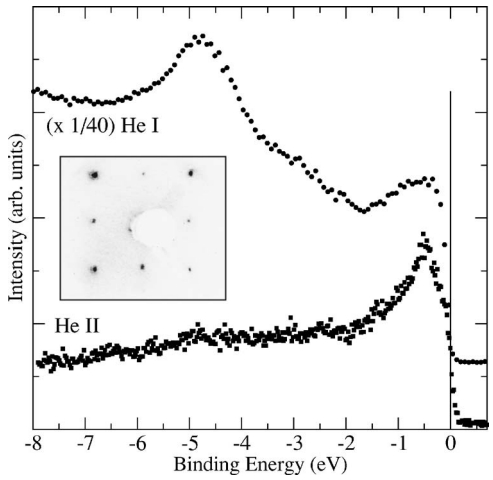

FIG. 7. He I (above) and He II (below) excited UPS spectra of $c(2\times2)$N/Fe(100). The inset reproduces the corresponding LEED pattern recorded at 40 eV. At this energy, the weaker spots reflect the $c(2\times2)$ superstructure.

The presence of excess of N in the subsurface (S-1) layer can be confirmed by comparison with UPS data for $c(2\times2)$N/Fe(100). Figure 7 shows the LEED pattern and UPS spectra recorded with He I and He II photon lines for Fe(100) covered with half a monolayer of N, which forms a $c(2\times2)$ superstructure. The geometry of this system has been determined experimentally: the adsorbed N atoms sit in the fourfold hollow sites of the Fe(100) surface, 0.27 Å above the plane of the surface Fe atoms, as determined by LEED.[23] The prominent peak at 0.6 eV and the weaker structure at 2.6 eV below the Fermi level are the well-known manifold of the *d* bands of bcc Fe.[24] The 2*p* states of the adsorbed N atoms appear in the spectrum recorded with He I (21.2 eV) photons as an intense peak at 5 eV below the Fermi level.[25] The adsorption geometry, charge transfer, and energy positions of both the N 2*p* level and the *d* states of Fe are reproduced by our first-principles calculations. Notice that the N 2*p* level at 5 eV recorded with He I photons is identical to the one observed in γ'-Fe_4N(100), but, contrary to γ'-Fe_4N, the UPS spectrum measured with He II (40.8 eV) photons shows only a barely detectable N 2*p* structure around −5 eV.

This fact reflects the competition between the increased surface sensitivity and the decreased relative photoionization cross section of the orbitals involved. The surface sensitivity increases with increasing photon energy due to the smaller mean free path of photoelectrons of the corresponding kinetic energy. On the contrary, the relative photoionization cross section of N 2*p* versus Fe 3*d* orbitals decreases upon increasing the photon energy (a factor of 4 when going from 21.2 to 40.8 eV).[26] The latter factor dominates, and the relative weight of the N 2*p* signal in the spectrum decreases. Thus, N atoms strictly confined to the *first* layer are weakly seen when using He II photons and the observation of a N 2*p* peak in γ'-Fe_4N indicates the presence of the N atoms in the subsurface layer that might drive the reconstruction.

The last piece of information is that the surface of γ'-Fe_4N is laterally inhomogeneous. This is proven by the

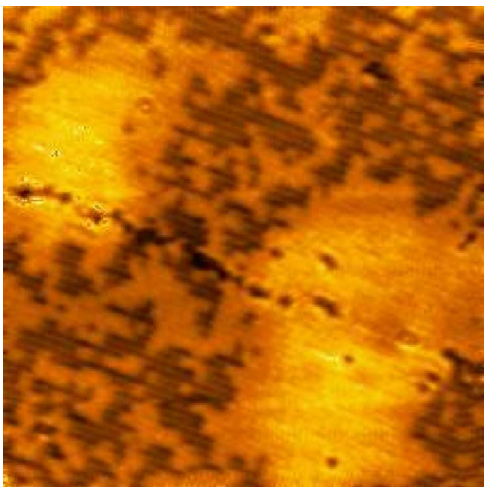

FIG. 8. (Color online) 200×200 Å^2 STM image of a 18-Å-thick γ'-Fe_4N film grown on Cu(100) at 700 K. The bias voltage was 0.3 V and the tunnel current was 1.45 nA. The image was recorded at 300 K.

STM image of Fig. 8, which shows that two kinds of regions can be detected on the surface upon zooming. The difference in corrugation between the brighter and darker areas of the surface is 0.6 Å. The high-resolution STM image shown in Fig. 9 proves that the darker patches show the characteristic weaving atomic arrangement of the $p4gm(2\times2)$ reconstruction, as described elsewhere,[7] while we proposed that the brighter areas that do not show atomic resolution in these conditions correspond to *unreconstructed* regions of the surface. Since an unreconstructed, bulk-terminated surface would give a $c(2\times2)$ LEED pattern with respect to the Cu(100) substrate[6] and all its spots will coincide with some of the diffraction spots of the $p4gm(2\times2)$ reconstruction, the LEED pattern observed in a surface containing reconstructed and unreconstructed patches will show only the $p4gm(2\times2)$ reconstruction.

The proportion of one and the other in a particular sample depends on the exact preparation procedure, i.e., on the precise amount of subsurface excess of N. This can be tuned by

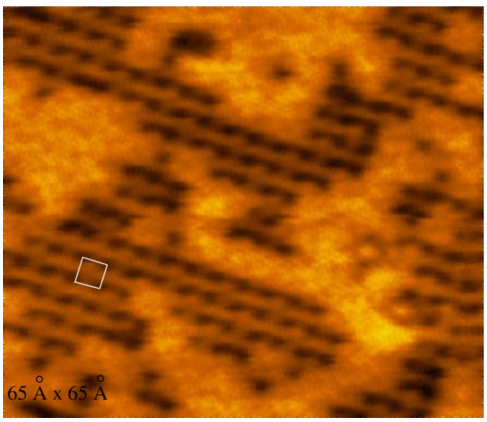

FIG. 9. (Color online) 65×65 Å^2 STM image of a 18-Å-thick γ'-Fe_4N film grown on Cu(100) at 700 K. The bias voltage was 0.3 V and the tunnel current was 1.45 nA.

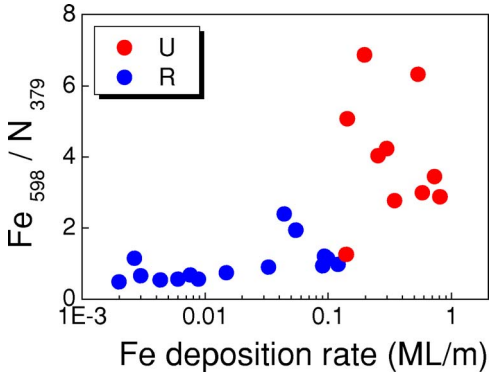

FIG. 10. (Color online) Ratio of the AES peaks of $Fe_5 98$ and $N_3 79$ for γ'-$Fe_4N(100)$ films as a function of the Fe deposition rate. Note that the value of the ratio of the AES peaks does not coincide numerically with the Fe/N stoichiometry. The blue points correspond to samples showing the $p4gm(2\times2)$ reconstruction and the red points show only the $c(2\times2)$ LEED pattern on bulk-terminated γ'-$Fe_4N(100)$. The reconstruction is associated with the excess of N in the subsurface layer.

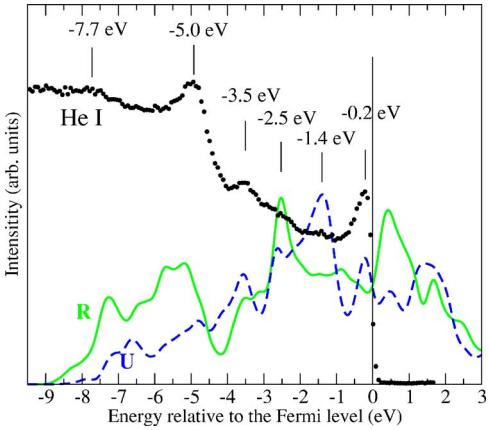

FIG. 11. (Color online) Comparison of the experimental UPS spectra recorded with He II (dots) on a 15-Å-thick γ'-Fe_4N film prepared at 700 K with the calculated DOS projected on the first two surface layers for γ'-$Fe_4N(100)$ films, unreconstructed and with ideal termination (U, blue dotted line) or $p4gm(2\times2)$ reconstructed due to excess of N in the subsurface layer (R, green continuous line).

the deposition rate of Fe. Figure 10 shows the ratio of the AES high-energy peaks of Fe and N as a function of the deposition rate of Fe (for constant N flux). Lower Fe deposition rates lead to smaller Fe/N AES ratio and reconstructed samples. Fe deposition rates above 0.2 ML/min lead to samples with smaller amount of N in the surface region and unreconstructed surface. Thus, a larger amount of subsurface N (detected also in the N 1*s* lower BE peak) corresponds to a larger fraction of $p4gm(2\times2)$ reconstructed surface. When the amount of the subsurface N is below a certain threshold, the $p4gm$ reconstruction is not detected.

Figure 11 shows that the self-consistent DOSs calculated for the unreconstructed and the $p4gm(2\times2)$ reconstructed γ'-$Fe_4N(100)$ surfaces are rather different. The large peak close to the Fermi level that appeared in the unreconstructed surface has shifted above it due to the reconstruction, while the main feature related to the occupied Fe states has shifted from −1.4 to −2.5eV. The N-related peaks in the −5 to −8eV region are much stronger in the reconstructed surface due to the subsurface N. The experimental UPS spectrum contains spectral features of both reconstructed and unreconstructed regions, since the actual surface contains the mixture of regions illustrated by the high-resolution STM images. The experimental peak close to the Fermi level and the weaker structures at −1.4 and −3.5 eV come from the unreconstructed patches, while the features at −2.5 eV and N-related peaks come from the $p4gm(2\times2)$ areas.

In conclusion, we have characterized the electronic structure of highly perfect, (100)-oriented films of γ'-Fe_4N epitaxially grown on Cu(100). A combination of photoemission, first-principles calculations, and STM is needed to reveal the electronic structure of this complex system. We have shown that the excess of N in the subsurface region detected by AES and suggested to be responsible for the $p4gm(2\times2)$ reconstruction recently reported[7] can be detected by UPS. The excess of N in the subsurface region may be a feature common to other iron nitrides, in view of the negative enthalpy of segregation (−110 kJ/mol) of N in Fe.

ACKNOWLEDGMENTS

This work has been supported by the Spanish CICyT (under Grants No. FIS 2004-01026, No. MAT2004-05865, and No. NAN2004-08881-C02-01) and the Comunidad de Madrid (under Grant No. S-0505/MAT-0194).

[1] J. M. D. Coey and P. A. I. Smith, J. Magn. Magn. Mater. **200**, 405 (1999).
[2] O. Kohmoto, IEEE Trans. Magn. **27**, 3640 (1991).
[3] J. L. Costa-Krämer, D. M. Borsa, J. M. Garcia-Martin, M. G. Martin-Gonzalez, D. O. Boerma, and F. Briones, Phys. Rev. B **69**, 144402 (2004).
[4] D. M. Borsa, S. Grachev, D. O. Boerma, and J. W. K. Kerssemakers, Appl. Phys. Lett. **79**, 994 (2001).
[5] J. M. Gallego, S. Y. Grachev, M. C. G. Passeggi, Jr., F. Sacharowitz, D. Ecija, R. Miranda, and D. O. Boerma, Phys. Rev. B **69**, 121404(R) (2004).
[6] J. M. Gallego, S. Y. Grachev, D. M. Borsa, D. O. Boerma, D. Ecija, and R. Miranda, Phys. Rev. B **70**, 115417 (2004).
[7] J. M. Gallego, D. O. Boerma, R. Miranda, and F. Yndurain, Phys. Rev. Lett. **95**, 136102 (2005).
[8] D. Ecija, E. Jimenez, J. Camarero, J. M. Gallego, J. Vogel, N. Mikuszeit, N. Sacristan, and R. Miranda, J. Magn. Magn. Mater. **00**, 000 (2006).
[9] W. Zhou, L-J. Qu, Q-M. Zhang, and D-S. Wang, Phys. Rev. B **40**, 6393 (1989).
[10] M. Sifkovits, H. Smolinski, S. Hellwig, and W. Weber, J. Magn. Magn. Mater. **204**, 191 (1999).

[11] S. Yu. Grachev, D. M. Borsa, and D. O. Boerma, Surf. Sci. **516**, 159 (2002).
[12] W. Kohn and L. J. Sham, Phys. Rev. **140**, A1133 (1965).
[13] J. M. Soler, E. Artacho, J. D. Gale, A. Garcia, J. Junquera, P. Ordejon, and D. Sanchez-Portal, J. Phys.: Condens. Matter **14**, 2745 (2002).
[14] J. P. Perdew, K. Burke, and M. Ernzerhof, Phys. Rev. Lett. **77**, 3865 (1996).
[15] N. Troullier and J. L. Martins, Phys. Rev. B **43**, 1993 (1991).
[16] L. Kleinman and D. M. Bylander, Phys. Rev. Lett. **48**, 1425 (1982).
[17] J. H. Onuferko, D. P. Woodruff, and B. W. Holland, Surf. Sci. **87**, 357 (1979).
[18] *Ex situ* x-ray diffraction has been performed using a six-circle diffractometer with optimized geometry for surface analysis placed on a rotatory anode, which produces Cu $K\alpha$ (8040 eV) radiation, and using the automatic attenuator system described in J. Alvarez, E. Paiser, and M. J. Capitan, Rev. Sci. Instrum. **73**, 2788 (2002).
[19] The peaks were fitted, after substraction of a Shirley background, with an assymmetric Doniach-Sunjic combination of Lorentzian and Gaussian line shapes.
[20] M. P. Seah and W. A. Dench, Surf. Interface Anal. **1**, 2 (1979).
[21] J. Alvarez, J. J. Hinarejos, E. G. Michel, J. M. Gallego, A. L. Vazquez de Parga, J. de la Figuera, C. Ocal, and R. Miranda, Appl. Phys. Lett. **59**, 99 (1991).
[22] B. C. Frazer, Phys. Rev. **112**, 751 (1958).
[23] R. Imbihl, R. J. Behm, G. Ertl, and W. Moritz, Surf. Sci. **123**, 129 (1982).
[24] M. Pessa, P. Heimann, and H. Neddermeyer, Phys. Rev. B **14**, 3488 (1976).
[25] W. Diekmann, G. Panzner, and H. J. Grabke, Surf. Sci. **218**, 507 (1989).
[26] At. Data Nucl. Data Tables **32**, 1 (1985). The cross sections for N $2p$ and Fe $3d$ at He I are 9.68 and 4.35 Mb, respectively. The cross sections for He II are 4.83 and 8.75 Mb, respectively.